CrossMark

Barth syndrome: Cellular compensation of mitochondrial dysfunction and apoptosis inhibition due to changes in cardiolipin remodeling linked to *tafazzin* (TAZ) gene mutation

François Gonzalvez [a,b,i,1], Marilena D'Aurelio [c,1], Marie Boutant [a], Aoula Moustapha [a], Jean-Philippe Puech [a], Thomas Landes [d], Laeticia Arnauné-Pelloquin [d], Guillaume Vial [e], Nellie Taleux [e], Christian Slomianny [f], Ronald J. Wanders [g], Riekelt H. Houtkooper [g], Pascale Bellenguer [d], Ian Max Møller [h], Eyal Gottlieb [i], Frederic M. Vaz [g], Giovanni Manfredi [c], Patrice X. Petit [a,*]

[a] INSERM U-747 et Université Paris V-Descartes, Centre de Recherche des Saint-Pères, 45 Rue des Saint-Pères, 75006 Paris, France
[b] Genentech, 1 DNA Way, MS 42, South San Francisco, CA 94080, USA
[c] Weill Medical College of Cornell University, 525 East 68th Street, A501, New York, NY 10021, USA
[d] Université de Toulouse, Centre de Biologie du Développement, CNRS UMR5547/Université Paul Sabatier, Toulouse, France
[e] Laboratoire de Bioénergétique Fondamentale et Appliquée, LBFA-INSERM U884, Université J. Fourier, 2280 Rue de la Piscine, 38041 Grenoble Cedex 9, France
[f] Laboratoire de Physiologie cellulaire, INSERM U800, Université des Sciences et Techniques de Lille 1, 59655 Villeneuve d'Ascq Cedex, France
[g] Department of Clinical Chemistry and Department of Pediatrics, Laboratory of Genetic Metabolic Diseases, University of Amsterdam, Academic Medical Center, Amsterdam 1105 AZ, The Netherlands
[h] Department of Molecular Biology and Genetics, Science and Technology Aarhus University, Forsøgsvej 1, DK-4200 Slagelse, Denmark
[i] Cancer Research UK, The Beatson Institute for Cancer Research, Glasgow G61 1BD, Scotland, UK

ARTICLE INFO

ABSTRACT

Cardiolipin is a mitochondrion-specific phospholipid that stabilizes the assembly of respiratory chain complexes, favoring full-yield operation. It also mediates key steps in apoptosis. In Barth syndrome, an X chromosome-linked cardiomyopathy caused by *tafazzin* mutations, cardiolipins display acyl chain modifications and are present at abnormally low concentrations, whereas monolysocardiolipin accumulates. Using immortalized lymphoblasts from Barth syndrome patients, we showed that the production of abnormal cardiolipin led to mitochondrial alterations. Indeed, the lack of normal cardiolipin led to changes in electron transport chain stability, resulting in cellular defects. We found a destabilization of the supercomplex (respirasome) $I + III_2 + IV_n$ but also decreased amounts of individual complexes I and IV and supercomplexes $I + III$ and $III + IV$. No changes were observed in the amounts of individual complex III and complex II. We also found decreased levels of complex V. This complex is not part of the supercomplex suggesting that cardiolipin is required not only for the association/stabilization of the complexes into supercomplexes but also for the modulation of the amount of individual respiratory chain complexes. However, these alterations were compensated by an increase in mitochondrial mass, as demonstrated by electron microscopy and measurements of citrate synthase activity. We suggest that this compensatory increase in mitochondrial content prevents a decrease in mitochondrial respiration and ATP synthesis in the cells. We also show, by extensive flow cytometry analysis, that the type II apoptosis pathway was blocked at the mitochondrial level and that the mitochondria of patients with Barth syndrome cannot bind active caspase-8. Signal transduction is thus blocked before any mitochondrial event can occur. Remarkably, basal levels of superoxide anion production were slightly higher in patients' cells than in control cells as previously evidenced via an increased protein carbonylation in the *taz1*Δ mutant in the yeast. This may be deleterious to cells in the long term. The consequences of mitochondrial dysfunction and alterations to apoptosis signal transduction are considered in light of the potential for the development of future treatments.

© 2013 Elsevier B.V. All rights reserved.

1. Introduction

Barth syndrome is a chromosome X-linked cardioskeletal myopathy and neutropenia (MIM 302060, BTHS). The disease is often fatal in infancy and early childhood, due to heart failure and bacterial infections [1,2]. Descriptions of this syndrome have been updated in review articles by Barth et al. [2] and Schlame and Ren [3], which defined Barth

syndrome as a mitochondrial disorder caused by an inborn error of phospholipid metabolism. Bione et al. [4] identified the gene responsible, the *tafazzin* (*TAZ*) gene, and mapped this gene to region q28 on the X chromosome. Phospholipid analyses of fibroblasts from patients and yeast *taz1* mutant cells showed cardiolipin levels to be low and revealed changes in acyl chain composition [5–7]. The *TAZ* gene modified in Barth syndrome seems to encode a transacylase essential for the terminal maturation of cardiolipin [7,8].

Cardiolipin [CL or bis-(1,2-diacyl-sn-glycero-3-phospho)-1′,3′-sn-glycerol] is a key mitochondrial membrane phospholipid [9] consisting of two glycerol-linked phosphatidyl moieties. The four acyl chains are usually mono- and di-unsaturated fatty acids in higher animals. Cardiolipin remodeling, by deacylation and successive reacylations, controls the final, specific acyl composition of the molecule. In mammals, CL is found specifically in the mitochondrial inner membrane, but tends to be concentrated at the mitochondrial contact sites [10] connecting the inner and outer membranes.

CL is associated with and modulates the activity of a number of key mitochondrial inner membrane enzymes involved in the respiratory chain (RC), including cytochrome *c* oxidase, carnitine palmitoyltransferase, creatine phosphokinase, the pyruvate translocator, mono-, di-, and tricarboxylate carriers, glycerol-3-phosphate dehydrogenase, the phosphate transporter, ATP/ADP translocase and ATP synthase [9,11]. CL may be seen as a sort of "glue" holding the mitochondrial respiratory chain together [12]. It is absolutely required for the activity of some of these respiratory enzymes and its interaction with mitochondrial proteins is specific, as enzyme activity is not fully reconstituted if it is replaced with other phospholipids [13]. Thus, as CL may regulate ATP generation in cells, the maintenance of appropriate amounts of CL in the mitochondria is essential for correct mammalian cell function. However, CL also plays a key role in many other cellular processes, including apoptosis [14,15]. There are currently several lines of evidence supporting the notion that mitochondria are autophagic substrates capable of shaping autophagic responses in several ways [16–18]. Recently, and of greater relevance to our work the physical state of the *tafazzin* lipid substrate (i.e., CL) has been shown to determine the transacylation specificity for *tafazzin* [19].

For death receptor-mediated apoptosis, activation of the mitochondrial pathway is required for apoptosis induction in "type II" cells, but not in "type I" cells. In type I cells, activation of the extrinsic pathway is sufficient to induce apoptosis. We are concerned here with the events leading to cell death in type II cells, i.e., the signals leading from death receptor stimulation to permeabilization of the outer mitochondrial membrane. Caspase-8 and Bid are the known procurers of the death signal in this part of the apoptotic pathway [20]. We previously showed that the mitochondrial surface becomes enriched in caspase-8 during type II extrinsic apoptosis, and that blocking the association of caspase-8 with the mitochondria inhibits p43–p10 formation, thereby preventing BID cleavage and blocking apoptosis [15]. The precise mechanisms for the insertion of active caspase-8 into the mitochondrial membrane remain unclear, although it has recently been shown that caspase-8 and Bid form a supramolecular complex on the mitochondrial membrane surface [15,21].

In the present study, we focused on the apparent compensation of abnormalities of mitochondrial metabolism in Barth syndrome lymphoblastoid cells (BTHS) [22]. No OXPHOS defect was observed at the cellular level. Despite decreases in the assembly of respiratory chain (RC) complexes and supercomplexes and an altered respiration associated with slight uncoupling observed in mitochondrial isolated and purified from such cells. These events were associated with slightly higher levels of superoxide anion production in patient derived lymphoblasts, which might be deleterious in the long term. We suggest that, in these cells, a compensatory increase in the number of mitochondria prevents the loss of mitochondrial respiration and ATP synthesis. We demonstrate that extrinsic apoptotic signaling in BTHS lymphoblasts is blocked at the mitochondria, because active caspase-8 could not interact with

mitochondria containing immature CL, nor with the remaining cardiolipin regardless of acyl chain composition nor with the monolysocardiolipins, which are present in very high amounts. The consequences of mitochondrial dysfunction and changes in apoptosis signal transduction are discussed in the light of possible future treatments.

2. Materials and methods

2.1. Cell culture and transfection

The lymphoblastoid cell lines were generated from two unrelated Barth syndrome patients (BTHS; DB105.2 and DB105.3, mutant cells) and two different controls (DB037, DB015.2, wild-type cells). They were a gift from R. Kelley (Johns Hopkins University School of Medicine, Baltimore, MD) and have been described elsewhere [23]. DB105.2 and DB105.3 have single point mutations in the *tafazzin* gene, resulting in substitutions (G197E and I209D, respectively) that inactivate the protein. These cells were immortalized ex vivo by Epstein–Barr virus infection. They were cultured in RPMI 1640 GlutaMAX I medium (GIBCO) supplemented with 10% fetal calf serum (FCS, Harlan), MEM vitamins, 0.5 mM sodium pyruvate, 10 mM HEPES and penicillin (50 IU/ml) plus streptomycin (50 μg/ml) (all from GIBCO). Other lymphoblast cell lines from Barth syndrome patients and control subjects were obtained from the Barth syndrome registry.

2.2. CL and MLCL analysis

Lipid analysis was performed as previously described [24]. Cells were sonicated for 20 s in PBS and phospholipids were extracted from an amount of homogenate equivalent to 1 mg of protein, as follows. We added 3 ml of 1:1 chloroform–methanol (v/v), followed by the internal standards (0.4 nmol tetramyristoyl-CL and 0.16 nmol dimyristoyl-phosphatidylglycerol (Avanti Polar Lipids)). This mixture was shaken vigorously and placed on ice for 15 min, after which it was centrifuged at 1000 $\times$g for 10 min. The supernatant was transferred to new tubes, and the protein pellet was re-extracted with 3 ml of 2:1 chloroform-methanol (v/v). The combined organic layers were evaporated under nitrogen at 45 °C. The residue was dissolved in 150 μl chloroform/methanol/water (50:45:5 v/v/v) supplemented with 0.01% NH$_4$OH, and 10 μl of the resulting solution was injected into the HPLC MS system (Thermo Electron Corporation). The column temperature was maintained at 25 °C. The lipid extract was injected onto a 2.1 $\times$ 250 mm silica column, with a 5 μm particle diameter (Merck). The phospholipids were separated from interfering compounds by a linear gradient of solution B (chloroform–methanol, 97:3, v/v) and solution A (methanol–water, 85:15, v/v). Solutions A and B contained 0.1 ml and 0.01 ml of 25% (v/v) aqueous ammonia per liter of eluent, respectively. The gradient (0.3 ml/min) was as follows: 0–10 min: 20% A/80% B to 100% A; 10–12 min, 100% A; 12–12.1 min: 100% A to 0% A; and 12.1–17 min, equilibration with 0% A. All gradient steps were linear, and the total analysis time, including equilibration, was 17 min. A splitter was inserted between the HPLC column and the mass spectrometer, and eluent was introduced into the mass spectrometer at a rate of 75 μl/min. A TSQ Quantum AM was used in the negative electrospray ionization mode. Nitrogen was used as the nebulizing gas. The source collision-induced dissociation collision energy was set at 10 V, the spray voltage used was 3600 V and the capillary temperature was 300 °C. Mass spectra of CL and MLCL molecular species were obtained by continuous scanning from m/z 400 to m/z 1000, with a scan time of 2 s. The spectra of CL and MLCL species were acquired at their retention times in the HPLC elution profile. The CL internal standard was set at 100% in each spectrum.

2.3. Induction and assessment of cell death

Cells were treated with the optimal concentration (0.5 μg/ml) of anti-Fas antibody (clone CH11, Beckton Coulter). Mitochondrial membrane

potential (DYm) and superoxide anion generation were evaluated by incubating cells for 15 min at 37 °C (5×10^5/ml) with 2.5 nM tetramethylrhodaminemethylester [TMRM, Molecular Probes, 1 mM stock solution in ethanol] for mitochondrial membrane potential determination or 1 mM hydroethidine (HE; Molecular Probes; 500 mM stock solution) for superoxide detection. Cells were gated on forward (FSC) and side (SSC) scatter to exclude debris. Fluorescence was elicited with an argon laser (excitation wavelength 488 nm) and recorded with a bandpass of 585 ± 20 nm (for TMRM and HE), and a red laser (635 nm) was used for TO-PRO-3 fluorescence for the simultaneous monitoring of cell viability (recorded with a 661 ± 16 nm bandpass). We analyzed at least 5×10^3 events with CellquestTM software (Becton-Dickinson), on a FACSCalibur cytometer. Intracellular K^+ concentration was measured by loading cells for 15 to 30 min with 2.5 μM cell-permeant benzofuran isophthalate acetoxymethyl ester (PBFI-AM; 500 μM stock solution in dimethylformamide). PBFI fluorescence was excited at 360 nm and evaluated at 485 ± 20 nm. The level of phosphatidylserine exposure on the outer plasma membrane was determined by staining cells with 1 mg/ml annexin V-FITC for 10 min at 4 °C (Beckman Coulter, Inc.). The pH within single cells was monitored with the fluorescent pH indicator 5-(and-6-)-carboxy-seminaphthorhodafluor-1 acetoxymethyl ester acetate (SNARF-1/AM) [25], which has an emission spectrum including two pH-sensitive bands: one corresponding to the protonated form (590 nm) and the other corresponding to the non protonated form (635 nm). Its pK is about 7.4, so pH changes in the 6.3 to 8.6 range can be determined by measuring the ratio of fluorescence at 635 nm to that at 590 nm. Cells were incubated in the culture medium for 20 min at 37 °C, under an atmosphere containing 5% CO_2, with 10 μM SNARF-1/AM (1 mM stock solution in DMSO), loaded with probe, washed and suspended in culture medium containing 25 mM Hepes (pH 7.4) for flow cytometry. An in vivo calibration curve of R versus intracellular pH was prepared as described by Thomas et al. [26]. Caspase activities were monitored with caspase-3 and caspase-8 detection kits (Calbiochem), according to the manufacturer's instructions. Briefly, cells were harvested and incubated for 30 min at 37 °C in the presence of a cell-permeant substrate: Red-DEVD-fmk (caspase-3) or Red-LETD-fmk (caspase-8). Cells were washed twice and analyzed by flow cytometry. Cells were also selected on the basis of viability, as estimated by double-staining with TO-PRO-3 (1 μg/ml; wit stock solution at 1 mg/ml). The level of phosphatidylserine exposure on the outer plasma membrane was measured by staining cells with 1 μg/ml annexin V-FITC for 10 min at 4 °C (Immunotech).

2.4. Electroloading of tBid

Cells were first resuspended at a density of up to 10^7/ml in an appropriate permeabilization buffer (PB; 10 mM phosphate buffer, 250 mM sucrose, 1 mM $MgCl_2$, pH 7.4) after centrifugation for 10 min at 100 $\times g$; 100 ml of cell suspension (10^6 cells) was placed between two flat stainless steel electrodes in parallel at the bottom of a Petri dish and voltage pulses were applied. The interelectrode distance was 0.5 cm. Electropulsation was carried out with a CNRS electropulsator (Jouan, France), which delivered square-wave pulses with independently adjustable electric pulse parameters (voltage, duration, number and frequency). Electric pulse parameters were monitored with a 15 MHz oscilloscope (Enertec, France). Cell electropermeabilization was performed at room temperature. Within 2 s of this process, fetal calf serum (Harlan) was added to the cell suspension at a final concentration of 20% (vol/vol). The cell suspension was then incubated for 10 min at 37 °C in an incubator containing 5% CO_2/95% air. Unless otherwise indicated, we then added 2 ml of complete culture medium to the cell suspension and incubated the cells at 37 °C in an incubator containing 5% CO_2/95% air until use [27]. tBid-electroloading efficiency was assessed immediately after electroloading, by immunofluorescence labeling. Control and electroloaded cells were suspended in 1 mM EDTA-containing phosphate-buffered saline (PBS), permeabilized with 0.2% Triton X-100 and fixed in 4% paraformaldehyde (PFA). Cells were then incubated with an anti-mouse Bid antibody (Santa Cruz), which was detected with an FITC-conjugated secondary antibody. Cell labeling was quantified in a FACS-Calibur 4C cytometer (FL-1 channel).

2.5. NAD(P)H and NADH determination

NAD(P)H fluorescence was elicited with a multiline ultraviolet light set at 400 mW on a FACS Vantage. Changes in the autofluorescence of normal and apoptotic cells were recorded as previously described by Gendron et al. [28]. The light emitted was collected with a 424 ± 40 nm bandpass for NAD(P)H fluorescence. The NADH content of the cell was also determined with the $NADH/NAD^+$ or the $NAD(P)H/NAD(P)^+$ Assay Kit (Cell Technology, Inc., Mountain View, CA, USA).

2.6. Transmission electron microscopy

Cell pellets were fixed by incubation with 2.5% glutaraldehyde in 0.1 M cacodylate buffer, pH 7.4 for at least 30 min at 4 μC. The fixed specimens were thoroughly washed in 0.1 M cacodylate buffer and then postfixed by incubation in 1% osmium tetroxide in the same buffer for 1 h at room temperature, stained en bloc with 2% uranyl acetate in distilled water for 15 min, dehydrated in a graded series of acetonitrile concentrations, and embedded in Epon resin. Ultrathin sections (80–100 nm thick) mounted on 150-mesh grids were stained with 2% uranyl acetate solution and Reynolds lead citrate.

2.7. Respiratory analysis for isolated mitochondria

The lymphoblastoid mitochondria were isolated and purified as previously described [29]. Lymphoblastoid cells (2×10^8 cells, about 11 ± 3 mg of protein) washed three times with medium A (100 mM sucrose, 1 mM EGTA, 20 mM MOPS (pH 7.4), 1 g/l BSA), were resuspended in 1 ml of medium B (medium A plus 10 mM triethanolamine, 5% Percoll, 0.1 mg/ml digitonin). After 3 min of incubation at 4 °C, the cells were disrupted with 7 strokes of a motor-driven (500 rpm) tightly fitting glass–Teflon pestle. The homogenate was centrifuged twice at 2500 $\times g$ for 5 min and the resulting supernatant was further centrifuged at 10,000 $\times g$ for 5 min. The mitochondrial pellet (about 1.4 ± 2 mg of protein) was resuspended in medium C (300 mM sucrose, 1 mM EGTA, 20 mM MOPS (pH 7.4), 1 g/l BSA, 1 mM PMSF). Oxygen uptake was measured using 100 μg of mitochondrial protein and calculated per mg of mitochondrial protein which was measured in medium D (300 mM mannitol, 10 mM KH_2PO_2 (pH 7.2), 10 mM KCl, 5 mM $MgCl_2$ and 1 g/l BSA) with a Clark oxygen electrode, in a 300 μl cell, with magnetic stirring, in which the temperature was kept at 37 °C by a thermostat. We used 1 mM succinate + 5 μM rotenone or 1 mM ascorbate + 500 μM TMPD as respiratory substrates. We added 70 μM ADP for the measurement of control respiration (CR). We added 10 μM FCCP for full uncoupling of respiration.

2.8. Respiratory chain analysis in whole cells

ATP synthesis was measured as described by Vives-Bauza et al. [30], with 2.0×10^6 cells, 0.04 mg/ml digitonin and pyruvate and malate as substrates (both used at a concentration of 1 mM). Oxygen consumption was measured in intact cells, with 1 mM pyruvate as the substrate, in the presence or absence of the uncoupler carbonyl cyanide *p*-trifluoromethoxyphenylhydrazone (FCCP, 1 μM), in an Oxygraph chamber equipped with a Clark-type electrode (Hansatech), at 37 °C, as described by D'Aurelio et al. [31]. Citrate synthase activity was measured in total cell lysates, as described by Trounce et al. [32].

2.9. AMP/ADP/ATP determination

Adenine nucleotides were separated by HPLC on a C18 column (Polaris 5C18-A, S250*4.6 Repl, Varian, France). The injection volume was 30 μl. The flow rate was 1 ml/min, and the cartridge was kept at 30 °C in a column oven. The mobile phase was 28 mM pyrophosphate buffer, pH 5.75. These compounds were detected on a spectrophotometer at a wavelength of 254 nm (L4200 UV Detector, Merck, USA). The retention times of ATP, ADP and AMP were 3, 5 and 9 min, respectively. Chromatograms were integrated with STAR software v.5 (Varian, France).

2.10. OPA-1 determination

For the assessment of OPA-1 oligomers, mitochondria were isolated as previously described [33] from DB037 and DB105-3 cells with and without incubation with 0.5 mg/ml anti-Fas antibody for 24 h. Mitochondria were incubated for 30 min at 37 °C with 10 mM EDC (Pierce) in PBS, and analyzed by SDS-PAGE (4%–12% bis-Tris acrylamide, Invitrogen), as described by Landes et al. [34]. Immunodetection was carried out with mouse antibodies against Hsp60 (LK2, Sigma) or cytochrome c (BD Biosciences) and rabbit antibodies against OPA-1.

2.11. Blue native-PAGE and SDS-PAGE

RC complex assembly was studied by BN-PAGE, as previously described [35]. Briefly, mitochondrial fractions obtained by treating the cells with 0.05–0.1% digitonin for 10 min were solubilized with 0.3–0.6% n-dodecyl β-D-maltoside (lauryl maltoside, LM) or 0.12–0.16% digitonin, for the identification of individual RC complexes and supercomplexes, respectively. For the immunodetection of protein complexes, we used monoclonal antibodies (Invitrogen) against the following subunits: 39 kDa subunit of complex I, 70 kDa subunit of complex II, core 2 of complex III, subunit I of complex IV and subunit β of complex V.

For SDS-PAGE studies, proteins from cell lysates resuspended in Laemmli sample buffer (BIO-Rad) were separated by SDS-PAGE, blotted and labeled with antibodies against the heat shock protein 60 (HSP60), (Stressgen), Mn-superoxide dismutase (MnSOD, Stressgen), subunit I of complex IV (COXI, Invitrogen), VDAC (Invitrogen), the 30 kDa of complex I (Invitrogen), and TIM23 (BD Biosciences). After incubation with the appropriate primary antibodies, all the blots were incubated with secondary antibodies conjugated to horseradish peroxidase (Jackson ImmunoResearch Laboratories, Inc.), for final detection with a Signal West Pico Chemiluminescent substrate (Thermo Scientific). Mitochondrial proteins were quantified by densitometric analyses of digitized Western blot bands, with Scion2 image software, and the results obtained are expressed as a percentage of WT.

2.12. Statistical analysis

For all assays, the values presented are the means of at least three independent measurements, unless otherwise specified. The statistical significance of differences between the WT and the mutant cells was estimated by unpaired two-tailed Student's t tests, with an asterisk indicating that $p < 0.05$.

3. Results

3.1. Electron microscopy of mitochondria in control and BTHS lymphocytes

As cardiolipin is specifically located in the mitochondrial inner membrane and more specifically at the contact sites between the two membranes, we investigated the effects of CL deficiency on the structural organization of lymphoblast mitochondria. In normal lymphoblasts, mitochondria were located essentially at two positions within the cell:

close to the plasma membrane and in the vicinity of the nuclear invaginations typically present in lymphoblasts (Fig. 1A). They contained groups of parallel cristae, which often extended across the entire body of the organelle (Fig. 1B and C). In BTHS lymphoblasts, there seemed to be more mitochondria (Fig. 1D), some of which appeared swollen and larger than those of control cells. BTHS mitochondria had a distinctive appearance, with major morphological changes and a markedly lower surface area of cristae. The cristae were no longer organized in parallel, appearing instead as round structures disconnected from the peripheral membrane (Fig. 1E and F). In some cases, they had a honeycomb-like structure (Fig. 1F square a) or adopted a lamellar, wrapped, curved form (Fig. 1F square b). Moreover, the mitochondrial membranes often enclosed electron-translucent areas devoid of cristae (Fig. 1E and F). A morphometric analysis of the electron micrographs confirmed that the average mitochondrial cross-section was larger in cells from patients than in control cells, and that the mitochondrial surface density was greater in cells from patients than in control cells (Table 1).

3.2. Analysis of CL and MLCL contents

A mass spectrometry comparison of control and BTHS lymphoblasts (Fig. 2A) showed that BTHS cells contained less mature cardiolipin (CL) and substantially more monolysocardiolipin (MLCL). Moreover, the acyl chains of the different CL species in Barth syndrome-derived cells were less unsaturated, as determined by mass spectrometry analysis, which showed a shift to higher m/z values within each cluster of CLs (Fig. 2B). The accumulating MLCL contained particularly large amounts of C18:1 and C16:0 acyl chains. These changes resulted in a complete reorganization of the fatty acid profile of CL in BTHS lymphoblasts. They also confirm that DB105.2 and DB105.3 cells presenting a single amino-acid substitution (G197E and I209D, respectively), display a deficiency of cardiolipin associated with the accumulation of substantial amounts of MLCL.

3.3. Respiratory activity of the isolated mitochondria

Polarographic studies were carried out to measure succinate (Fig. 3A) and ascorbate/TMPD (Fig. 3B) respiration levels in control and patient-derived lymphoblastoid mitochondria. Control mitochondria oxidized succinate ($+$ rotenone) at a rate of about 60 nmol O_2 min^{-1} mg^{-1} protein, with a control respiration (RC) of about 2.2 after the addition of ADP, whereas mitochondria from patients had a low oxidation rate (26 nmol O_2 min^{-1} mg^{-1} protein) and a lower RC, suggesting lower levels of coupled electron transport activity (Fig. 3A). Similar results were obtained for the oxidation of ascorbate $+$ TMPD (Fig. 3B), demonstrating lower levels of respiration in mitochondria from patient-derived cells than in control mitochondria, associated with modified coupling between electron transport and phosphorylation. Curiously, the uncoupled respiratory capacity measured with both substrates was the same in the mitochondria from both patients and normal individuals.

3.4. Respiratory chain assembly in BTHS and control lymphoblasts

CL is known to be a critical component of the inner mitochondrial membrane, responsible for stabilizing the assembly of inner membrane protein complexes. We analyzed the assembly of RC complexes in BTHS and control lymphoblasts, by blue native polyacrylamide gel electrophoresis (BN-PAGE). The optimal conditions for mitochondrial complex isolation and solubilization were determined by titration with various amounts of digitonin (DG) and lauryl maltoside (LM), respectively (Fig. 4A). Individual complexes I, III and V were best resolved with 0.05% DG and 0.6% LM, whereas individual complex IV was best resolved with 0.1% DG and 0.6% LM. In these conditions, mutant cells displayed lower levels of assembled complexes I, IV (Fig. 4A panel 1 and table below), and V (Fig. 4A panel 2 and table below) than controls. In the presence of 0.3% LM, a partial I $+$ III supercomplex
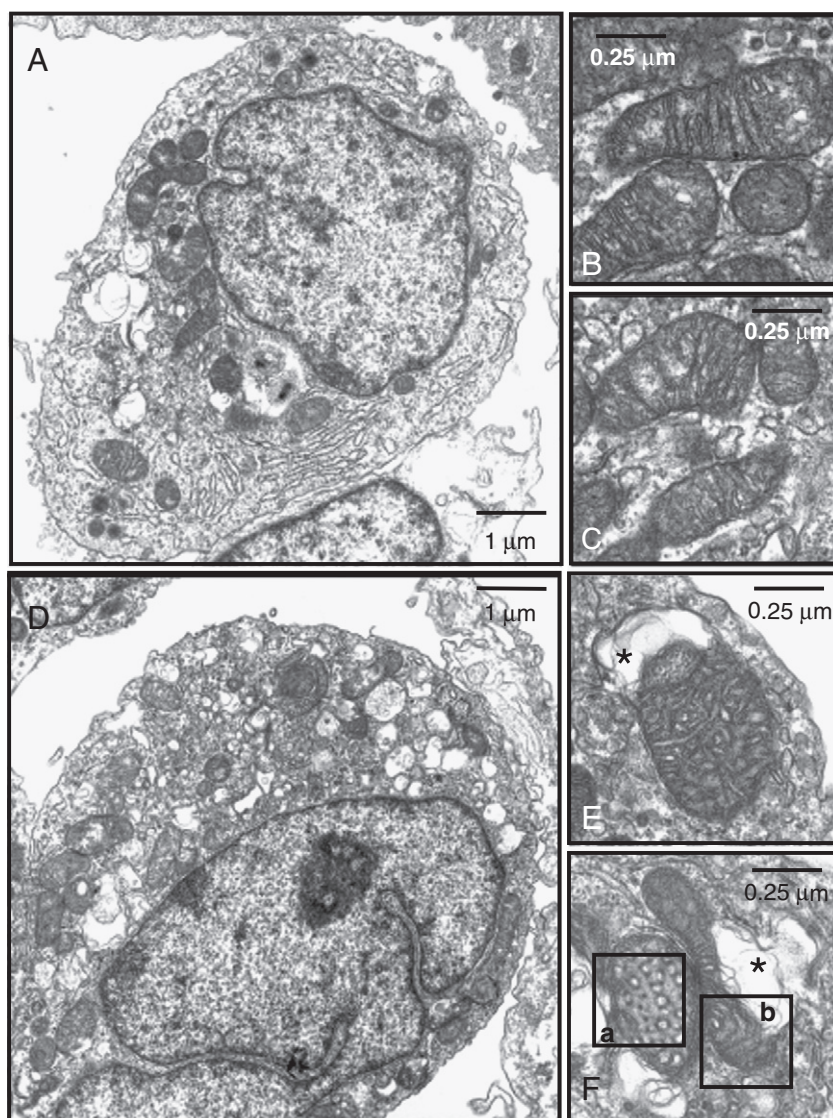
Fig. 1. Electron micrographs of mitochondria from lymphoblasts from controls and BTHS patients. (A) Control lymphoblasts (DB037). (B) and (C) Structure of mitochondria from control lymphoblasts (DB037). (D) Lymphoblasts from a patient (DB105-3). (E) and (F) Structure of mitochondria from the lymphoblasts of a patient (DB105-3). * Electron-translucent area surrounded by the outer mitochondrial membrane (or a membrane derived from it).

was detected in control, but not in BTHS cells. With 0.6% LM, the I + III supercomplex in control cells was incompletely resolved, but nonetheless better resolved into its individual complexes. Supercomplex III + IV levels were lower in BTHS cells than in control cells. No difference between mutant and WT cells was observed for the assembly of complexes II and III.

Table 1
Morphometric analysis of lymphoblast mitochondria by transmission electron microscopy.

Cell type	Mitochondria	Mitochondrial surface density	
	Mitochondrial cross-section (number per cell)	Percentage in the cytoplasm	Percentage in whole cells
Control 037	12 ± 3	8.1 ± 0.8	5.4 ± 0.9
Control 015-2	13 ± 3.5	8.0 ± 1.2	5.3 ± 0.7
Patient 105-3	26 ± 5*	15.1 ± 2.4*	10.1 ± 1.9*
Patient 105-2	24 ± 4.9*	14.9 ± 2.5*	9.8 ± 1.7*

* Asterisks indicate a significant difference between control DB037 and patient-derived lymphoblasts DB105-3 ($p < 0.05$).

RC complexes I, III and IV are organized into functional supercomplexes ($I + III_2 + IV_n$) [35]. We therefore investigated whether the supermolecular organization of the RC was affected in mutant cells. Mitochondrial samples obtained after two-step digitonin solubilization were analyzed by BN-PAGE (Fig. 4B). Supercomplexes $I + III_2 + IV_n$ were best resolved with 0.16% DG, and were present in smaller amounts in BTHS cells (54% of control).

Western blotting of SDS-PAGE gels of total cell lysates showed lower steady-state levels of the 30 kDa subunit of complex I and of cytochrome c oxidase subunit I (COXI) (Fig. 4C) in the mutant cells than in the WT cells, consistent with the observed lower level of the assembly of complexes I and IV.

3.5. OPA-1 status is not affected by TAZ gene defects

It has recently been suggested that OPA-1 controls cytochrome c mobilization by forming local oligomers at crista junctions [36,37]. The stability of OPA-1 complexes may therefore be affected by the CL environment. Mitochondria isolated from WT (DB037) and patient-derived lymphoblasts (DB105-3) contained similar amounts of OPA-1 oligomers (Fig. 5). OPA-1 complex disassembly and a loss of cytochrome
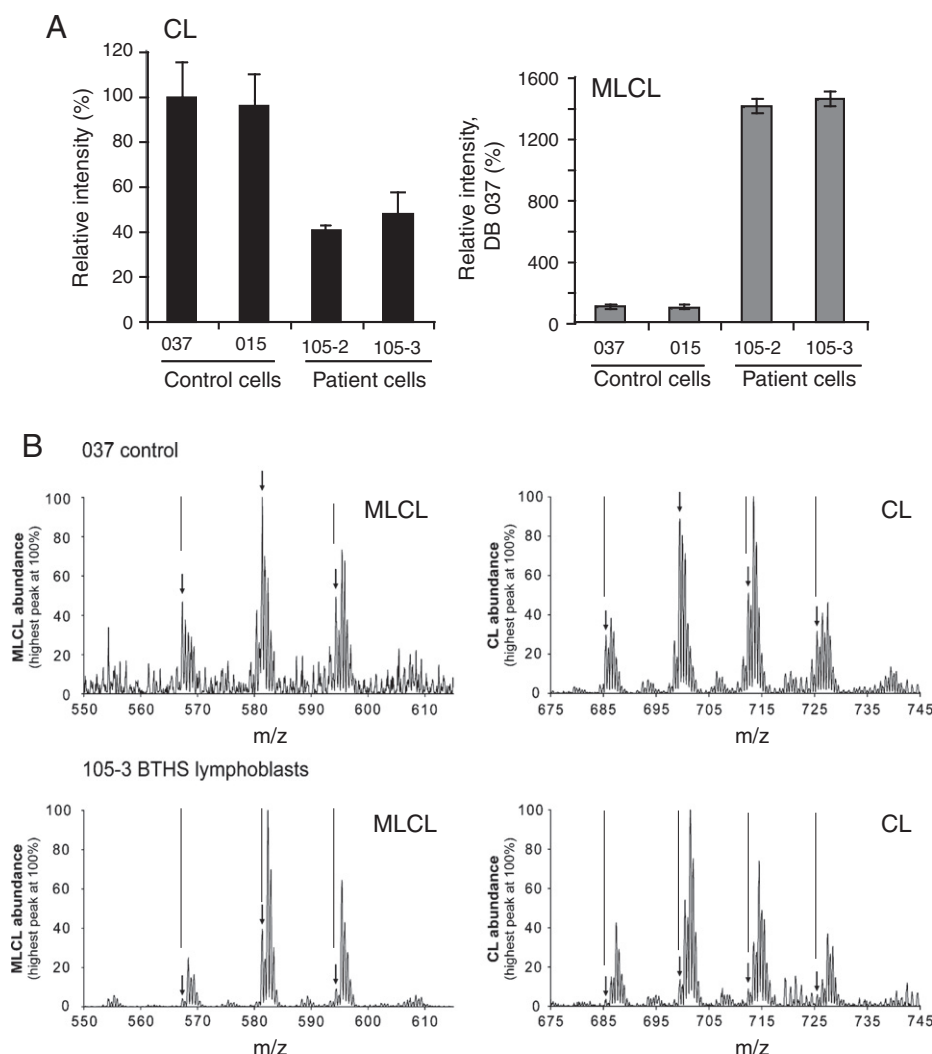
Fig. 2. Analysis of cardiolipin (CL) and monolysocardiolipin (MLCL) from control (DB037/DB015) and BTHS lymphoblasts (DB105-3/DB105-2).

c were observed in DB037 cells treated with anti-Fas antibody (Fig. 5). By contrast, no disruption of OPA-1 oligomers or cell death was observed in lymphoblasts from patients (Fig. 5). These observations suggest that BTHS cells may maintain OPA-1 complexes, possibly accounting for their capacity to resist apoptosis. The stability of the OPA-1 complexes did not seem to be affected by the changes in CL structure or the amount of CL observed in the mutant (Fig. 2).

3.6. Bioenergetic state of BTHS and control lymphoblasts

We investigated whether the decrease in the amount of RC super-complexes affected mitochondrial function and oxidative phosphorylation (OXPHOS), by investigating ATP synthesis and mitochondrial respiration. No difference in ATP synthesis or mitochondrial respiration was found between mutant and WT cells when the rates were expressed per mg of protein (Table 2). Citrate synthase, an enzyme of the mitochondrial matrix used as a marker of the mitochondrial content, was found to be significantly increased in BTHS cells (Table 2). These results suggest that BTHS cells had a greater mitochondrial content than control cells. HPLC determinations on cell lysates showed that ATP/ADP ratio was slightly lower in BTHS cells than in control cells (Fig. 6A). [AMP] is proportional to the square of [ADP] divided by [ATP] (assuming close equilibrium with adenylate kinase in most cells). Thus, if the absolute ATP and ADP (Fig. 6A) levels are taken into account, together with [AMP], [AMP] is clearly higher in BTHS cells than in control cells (Fig. 6B). This

finding is of particular importance, because an increase in AMP/ATP ratio (from 0.078 in control to 0.103 in patient-derived cells) might lead to the activation of AMP kinase, a major regulator of mitochondrial biogenesis via the PGC1-alpha pathway, accounting for the observed increase in mitochondrial mass. Furthermore, the NADH content of BTHS lymphoblasts was higher than that of controls (Fig. 6C), suggesting that this compound is not readily oxidized by the RC in the mitochondria of these cells, most likely because of the deficit in complex I.

3.7. Flow cytometry analysis of the early events of apoptosis in control and BTHS lymphoblasts

We investigated LETD cleavage in control cells and cells from patients, in the presence (αCD95) and absence of apoptotic stimuli. The triggering of apoptosis in control lymphoblasts led to the activation of caspase-8 and cleavage of the LETD substrate (Fig. 7A). No such cleavage activity was observed when the same experiment was carried out with lymphoblasts from patients (Fig. 7A).

The collapse of mitochondrial membrane potential ($\Delta\Psi$m) is one of the first changes to occur in apoptosis [6,7]. We therefore investigated the temporal relationship between the loss of $\Delta\Psi$m and NAD(P)H oxidation. Control cells and BTHS cells were labeled with TMRM, to obtain information about $\Delta\Psi$m changes (Fig. 7B). The treatment of cells with αCD95 for 24 h decreased $\Delta\Psi$m in a significant proportion (65%) of control cells (Fig. 7B). Apoptosis was almost totally inhibited in BTHS
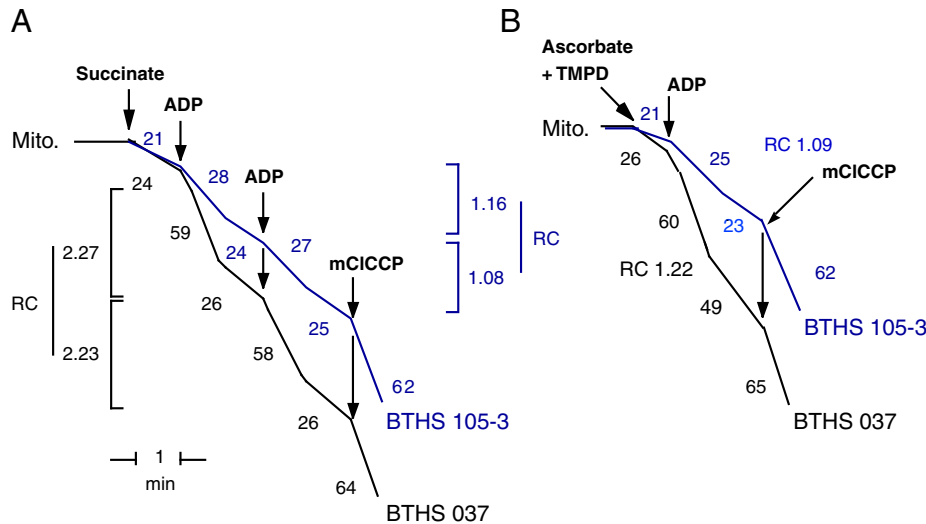
Fig. 3. Respiratory activities of mitochondria isolated from control (DB037) and patient-derived lymphoblasts (DB105-3). Dark line, the respiration of control lymphoblasts (DB037) and blue line, the respiration of the patient-derived lymphoblasts (DB105-3). Succinate (in the presence of rotenone) oxidation (left) and ascorbate + TMPD oxidation (right). Concentrations used: 2 mM succinate, 5 μM rotenone or 1 mM ascorbate + 500 μM TMPD; 70 μM ADP and 5 μM mClCCP. The oxidation rate indicated alongside the trace is given in nmol O_2 ml^{-1} mg^{-1} protein. (A) CL composition of cell lines derived from the cells of controls (DB015/DB037) and patients (DB105-2/105-3). The data for MLCL are expressed as a percentage (%) of the MLCL levels measured in the control. (B) Detailed profile of the CL and MLCL present in control (037) and patient-derived cells (105-3): The arrows marking the peaks in control samples indicate the various CL and MLCL m/z. A clear shift in m/z (below) indicates a change in fatty acyl chain saturation in the samples from the patient. The observed CL clusters (I–V) are: I = 66 carbon atoms; II = 68 carbon atoms; III = 70 carbon atoms; IV = 72 carbon atoms (likely 4 × 18); and V = 74 carbon atoms. Each peak within a given cluster represents the saturation level of the acyl chains ranging from 2 (right) to the maximum 8 (left) double bonds.

lymphoblasts as shown by comparison with control cells (Fig. 7B, compare the lower right and lower left panels).

As ΔΨm dissipation is associated with NAD(P)H oxidation, we investigated the NAD(P)H status of both control and BTHS lymphoblasts. The fluorescence of reduced pyridine nucleotides (NADH and NADPH) accounts for most of the autofluorescence of cells induced by illumination with near-UV light, and this autofluorescence is generated almost exclusively by the mitochondria. Oxidized pyridine nucleotides (NAD$^+$ and NADP$^+$) are not fluorescent. Changes in autofluorescence therefore reflect changes in the redox state of pyridine nucleotides. The absence of a significant difference in pyrimidine nucleotide oxidation ([NAD(P)H]) between control and BTHS lymphoblasts and the data for NADH determination demonstrated that NADH levels were higher in cells from patients (Fig. 7C). We also monitored the oxidation of pyridine nucleotides early in apoptosis, by analyzing control and BTHS lymphoblasts incubated with and without αCD95 for 24 h. In most control cells, NAD(P)H-dependent autofluorescence was decreased by treatment for 24 h with αCD95 (Fig. 7C). However, this was not the case in cells derived from patients, in which all these phenomena were inhibited.

3.8. Other cell death characteristics abolished in BTHS lymphoblasts

Multiparameter analyses (Fig. 7) showed that most cells (77%) were depleted of NAD(P)H well before any increase in the generation of superoxide anions could be detected by hydroethidine (HE) staining (only observed in 60% of cells; Table 3b). Caspase-3 activity was associated with control cell apoptosis (Table 3a), but was abolished in cells from the patient. Similarly, intracellular pH, as determined with the fluorescent pH indicator SNARF-1AM, decreased in most control cells after stimulation with aCD95 (Table 3a), but no change was recorded in cells from patients, even after treatment with αCD95. We also investigated intracellular K$^+$ content (Table 3a) and the level of phosphatidyl serine residue exposure at the plasma membrane, by annexin-V FITC staining (Table 3a). The data obtained confirmed that control lymphoblasts underwent a normal apoptotic process, with the late occurrence of K$^+$

efflux and PS exposure, whereas BTHS cells were not affected by Fas (αCD95).

Careful examination of the control and BTHS lymphoblasts might reveal more subtle changes, even if apoptosis is undetectable in BTHS cells. Following HE staining, basal levels of superoxide anion production were reproducibly higher in BTHS cells (mean fluorescence: 16 ± 0.9 AU; Table 3b, patient 105-3) than in control cells (mean fluorescence: 8.4 ± 1.2 AU; Table 3b, control DB037).

3.9. Efficacy of tBid and caspase-8 binding to isolated mitochondria from control and BTHS lypmphoblasts

Apoptosis thus appears to be blocked at the mitochondrial level, at a point before any decrease in mitochondrial membrane potential can be measured or any change linked to the activation of apoptosis through caspase-8, such as NAD(P)H reduction or caspase-3 activity, can be detected. Before assessing caspase-8 binding and activity at the mitochondrial membrane, we evaluated the electropermeabilization by tBid in control and BTHS lymphoblasts (Fig. 8). The introduction of tBid-FITC, by electroloading, into control or BTHS lymphoblasts resulted in similar staining patterns (Fig. 8A). Moreover, tBid induced apoptosis and necrosis in both control and BTHS cells (Fig. 8B and C). An analysis of the effect of introducing tBid into control (Fig. 8B) and BTHS (Fig. 8C) lymphoblasts revealed that the BTHS lymphoblasts were more sensitive to cell death induction (Fig. 8C). The decrease in mitochondrial membrane potential affected 70% of BTHS cells after 2 h, but only 40% of control lymphoblasts. BTHS cells were also more sensitive to both apoptosis and necrosis (≥80% of the lymphoblasts being affected at 4 h, whereas ≥60% of the control cells died). There was also a marked shift from an apoptotic phenotype to a necrotic phenotype in BTHS cells, during longer periods of incubation with exogenous tBid (Fig. 8C).

Caspase activation often involves the formation of triggering complexes or an activation platform. Many such complexes have been identified in the vicinity of the plasma membrane: the DSC for caspases-8 and -10 [38], the apoptosome for caspase-9 [39] and, more recently, for caspase-8 [15], which seems to be inserted into the mitochondrial
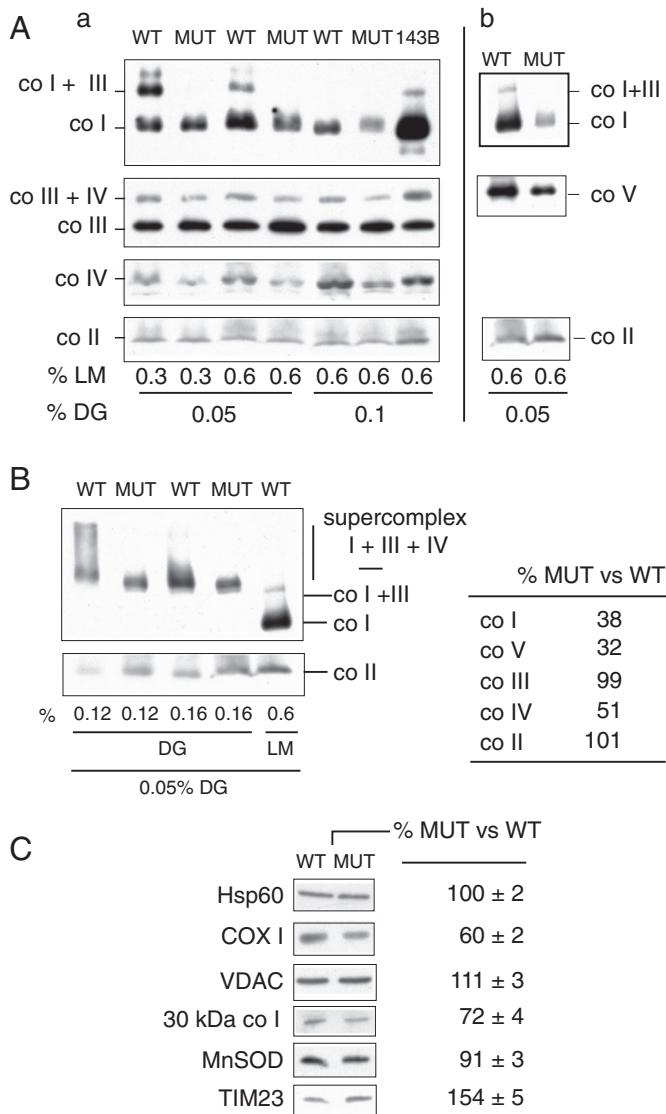
Fig. 4. Destabilization of the respiratory supercomplexes in lymphoblasts from Barth syndrome patients. (A) Panel 1: BN-PAGE of RC complexes. WT, 037 cell line; MUT, 105-3 cell line; 143B, osteosarcoma cell line; coI, complex I; coII, complex II; coIII, dimer of complex III; coIV, complex IV. The amounts of detergent are indicated below each lane. Panel 2: same conditions as in panel 1 in an independent BN-PAGE experiment probed with anti-complex V antibody. A separate gel was necessary to detect complex V (coV) because the band co-migrates with complexes III + IV. RC levels in MUT cells are expressed as a percentage of WT, estimated by densitometry of bands of complexes solubilized with 0.05%DG + 0.6%LM for all complexes except complex IV (0.1%DG + 0.6%LM) from at least three independent experiments, and are indicated in the table below. (B) BN-PAGE of RC supercomplexes. I + III$_2$ + IV$_n$, RC supercomplexes containing complex I monomer, complex III dimer and complex IV in various proportions. (C) Mitochondrial protein levels. Western blot of whole-cell lysates separated by denaturing SDS-PAGE, blotted, and probed with the specific antibodies indicated on the left. The amount of mitochondrial protein, expressed as a percentage of WT, estimated by the densitometry of Western blot bands, is indicated on the right. ± SD calculated on 6 gels.

4. Discussion

4.1. There are fewer respiratory complexes, but higher levels of respiration in BTHS cells

The two ATP-regenerating systems within cells adapt to the needs of the cell. These two systems are the phosphorylation of ADP, using the high-energy intermediates generated in the glycolytic pathway, and oxidative phosphorylation in mitochondria, which involves the proton motive force. These two processes must be coordinated and the total ATP turnover of the cells must closely match actual requirements during growth and differentiation, and the activation and performance of various cellular functions. The free energy, ΔG, of ATP hydrolysis depends principally on the ATP/ADP ratio. In general, with high energy turnover, this ratio remains remarkably stable. For example, in heart muscle, it is practically independent of workload and, thus, of ATP turnover [40]. Most of the cell's ATP is generated by mitochondrial oxidative phosphorylation. The mitochondrial respiratory chain comprises a number of
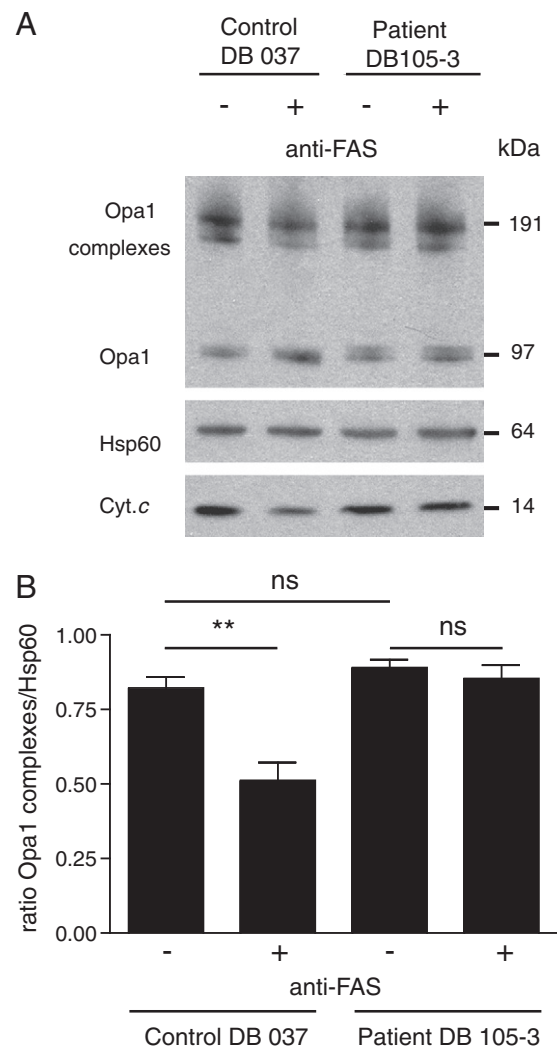

Fig. 5. OPA-1 sensitivity to apoptosis and CL dysfunction. (A) Mitochondria isolated from DB037 or DB105-3 cells incubated for 24 h with anti-FAS antibodies (+) or in the absence of these antibodies (−) were cross-linked and analyzed by Western blotting with the antibodies indicated on the left of the panels. [B] Levels of OPA1 oligomers were measured by densitometry with ImageJ software, with normalization against a loading control, Hsp60. Tukey's test was used for statistical analysis (non significant: $p > 0.05$; significant, **, $p < 0.01$), and the means ± SEM of three independent experiments are shown.

membrane in its active form. We therefore investigated the selectivity of the interaction between active caspase-8 and isolated mitochondria from control and BTHS lymphoblasts (Table 4). Active caspase-8 was clearly detected to be bound to the mitochondrial membrane of control lymphoblasts, but not to the mitochondrial membrane of BTHS lymphoblasts. This binding appeared to be specific, because the fluorescence associated with isolated control mitochondria was abolished by addition of the pan-caspase inhibitor Bod-D-fmk or Z-IETD-fmk, which is more selective for caspase-8.

Table 2

Respiratory chain analysis measured on intact cells. ATP synthesis activities, oxygen consumption in the absence (coupled respiration) or presence (uncoupled respiration) of FCCP and citrate synthase activity (CS). The values shown are means of at least three independent measurements expressed in nmol/min/mg protein. Statistically significant differences between control (control 037) and BTHS patient-derived lymphoblasts (patient 105-3) are indicated: *** = $p < 0.0005$, ** = $p < 0.005$, * = $p < 0.05$.

Activities nmol/min/mg	ATP synthesis	Coupled respiration	Uncoupled respiration	Citrate synthase (CS)
Control 015	22.7 ± 1.1	7.5 ± 0.6	17.8 ± 0.8	162.3 ± 21.8
Patient 105-3	21.8 ± 1.1	7.1 ± 0.9	17.9 ± 2.7	263.2 ± 9.0***

	ATP/CS	Coupled/CS	Uncoupled/CS
Control 015	0.14 ± 0.007	0.05 ± 0.004	0.11 ± 0.005
Patient 105-3	0.09 ± 0.005**	0.03 ± 0.004*	0.08 ± 0.011*

membrane-bound enzyme complexes, which transfer electrons from NADH to oxygen, ultimately producing water and generating a proton gradient across the inner mitochondrial membrane. Electrons from NADH are initially transferred, via complex I (NADH:ubiquinone oxidoreductase) and ubiquinone, to complex III (ubiquinol: cytochrome *c* oxidoreductase). They then pass through the peripheral electron carrier cytochrome *c* and complex IV (cytochrome *c* oxidase) to the terminal acceptor, molecular oxygen. The electrochemical proton gradient generated is used by complex V ($F_O F_1$-ATP synthase) to produce ATP. The respiratory chain complexes may be organized into multienzyme assemblies, known as supercomplexes. Such a supercomplex, consisting of complex I, dimeric complex III, and a variable number of complex IV units, has been visualized as a 3D map generated by random conical tilt electron microscopy analysis [41]. The ubiquinone and cytochrome *c* binding sites of each complex can be seen within the supercomplex, located close to the site of binding to the next complex in the respiratory chain. These findings provide structural evidence for direct substrate channeling in supercomplex assembly, with short diffusion distances for mobile electron carriers.

A destabilization of respiratory chain supercomplexes, accompanied by a decrease in the amounts of individual complexes I, IV and V, was observed in BTHS cells (Fig. 4). These results confirm previous findings for Barth syndrome cells [42] and are consistent with the hypothesis that higher levels of electron transfer complex organization into supercomplexes are dependent on CL. The decreased levels of complex V (resolved with detergent lauryl maltoside, Fig. 4A panel 2) is interesting, since this complex is not part of the supercomplex. The decrease suggests that cardiolipin is required not only for the association/stabilization of the complexes into supercomplexes but also for the modulation of the amount of individual respiratory chain complexes.

Mitochondria from patients with Barth syndrome have a lower CL content than control cells and also display changes in acyl chain composition (Fig. 2). Supercomplex destabilization would be expected to result in electron transport defects [35]. Interestingly, isolated mitochondria from patient's cells, display lower rates of coupled respiration but unchanged uncoupled respiration as compared to mitochondria from cells from normal individuals (Fig. 3). This indicates that the altered CL content (Fig. 2) and the decreased amount of respiratory complexes and super-complexes (Fig. 4) are only limiting for the biologically relevant coupled respiration. BTHS cells show changes in mitochondrial structure (Fig. 1) (also described by Acehan et al. [43]), in cardiolipin composition (Fig. 2), and in the respiratory properties of isolated mitochondria (Fig. 3), but unchanged respiration rates (Table 2) and similar ATP/ADP ratios (Fig. 6). Thus, despite the problems caused by lower levels of CL and fatty acid chain modifications, BTHS lymphoblasts can, nonetheless, fulfill their energy demand by a compensatory increase in mitochondrial mass, as shown by electron microscopy (Fig. 1 and Table 1) and citrate synthase activity (Table 2).
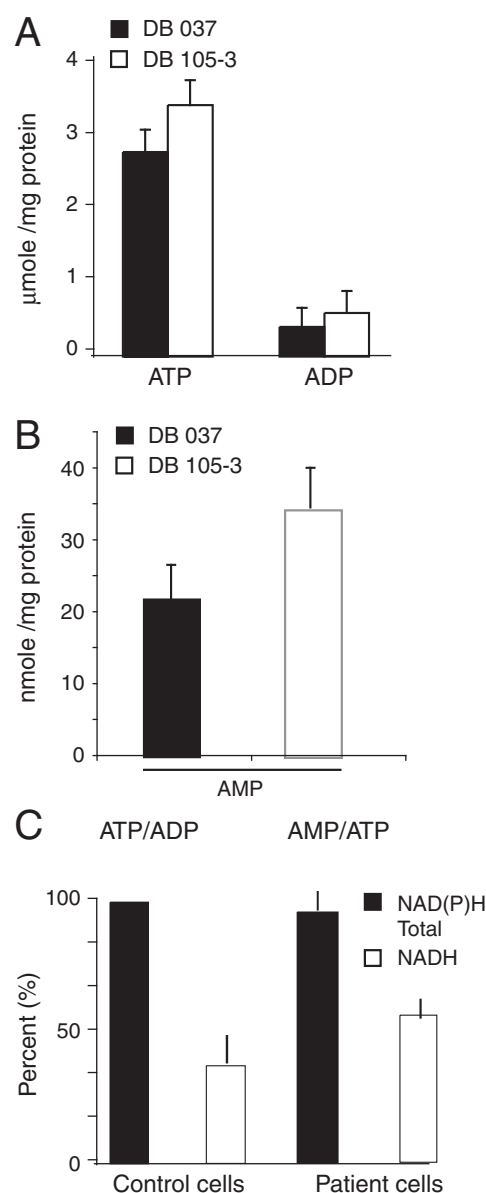
Fig. 6. AMP/ADP/ATP content and pyrimidine nucleotide determination in control and BTHS lymphoblasts. (A) Determination of the ADP and ATP contents of control lymphoblasts (DB037) and of Barth syndrome patient-derived lymphoblasts (DB105-3). (B) AMP content of control (DB037) and of Barth syndrome patient-derived lymphoblasts (DB105-3). (C) NAD(P)H and NADH determinations in control (DB037) and Barth syndrome patient-derived lymphoblasts (DB105-3). The 100% NAD(P)H represent 75 ± 5 nM per 6×10^5 cells whereas 100% NADH corresponds to 5 ± 2 nM per 6×10^5 cells.

4.2. OPA-1 oligomer formation is not affected by the change in CL structure in BTHS cells

OPA-1 status did not seem to be affected in BTHS cells (Fig. 5), despite expectations of a destabilization of OPA-1 complexes due to the changes in mitochondrial morphology observed on electron microscopy. OPA-1 oligomer formation and GTP hydrolysis have been shown to be increased by cardiolipin [17]. We anticipated a possible destabilization of OPA-1 complexes due to the smaller amount of CL present and the modifications to the acyl chains of CL molecules, but we found no difference in OPA-1 complex formation between control and BTHS lymphoblasts (Fig. 5). This suggests that CL acyl chains, which are clearly more saturated in patient-derived cells, are not involved in OPA-1 complex formation.
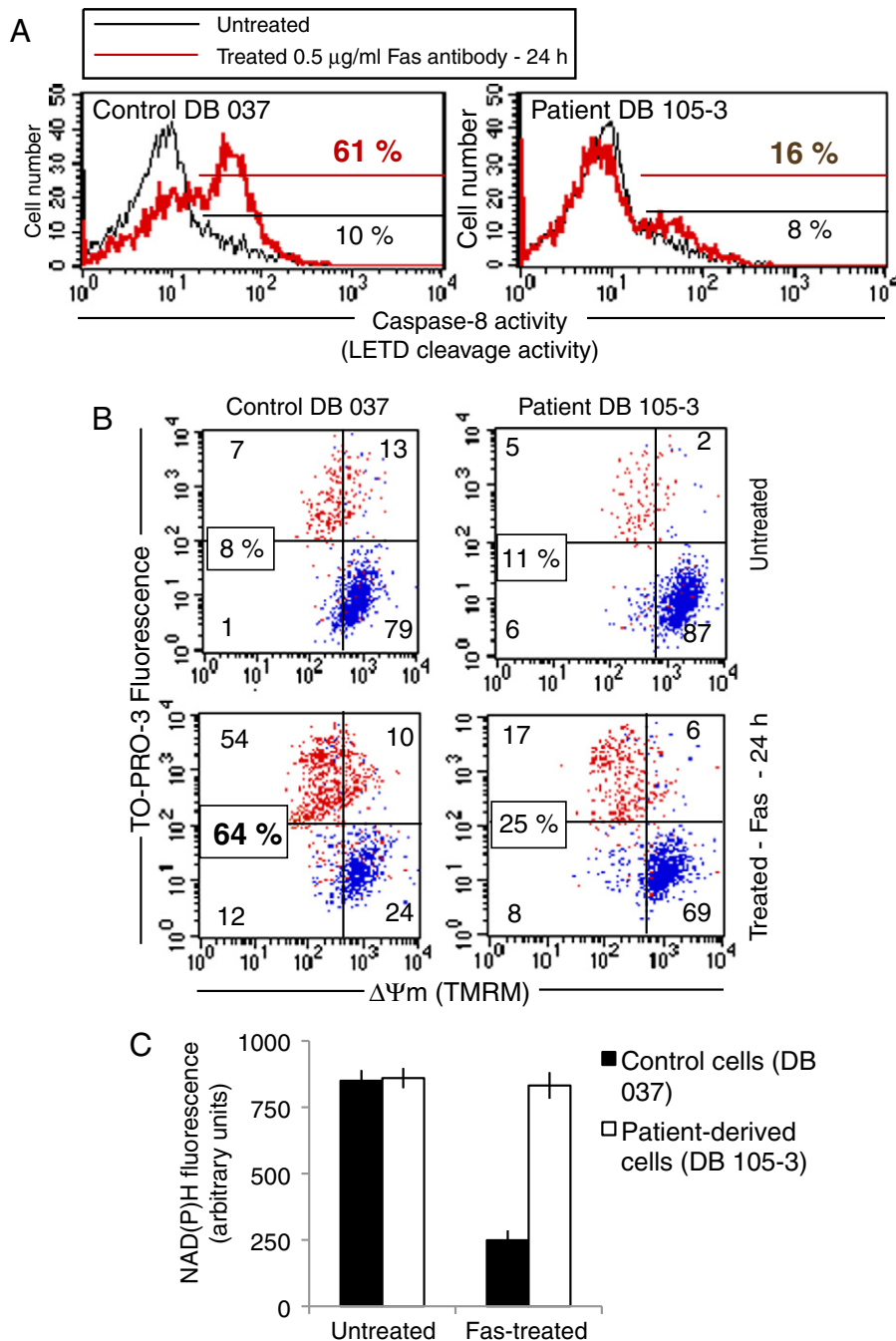
Fig. 7. Flow cytometry analysis of early apoptotic events in control and BTHS lymphoblasts. Lymphoblasts were incubated for 24 h with or without 0.5 mg/ml Fas antibody, and the following were assessed: (A) caspase-8 activity, as measured by LETD cleavage activity. (B) Mitochondrial membrane potential assessed on the basis of TMRM and cellular viability (TO-PRO-3) and (C) NAD(P)H fluorescence.

OPA-1 proteolysis during apoptosis has been linked to a decrease in $\Delta\Psi m$ and mitochondrial fusion, leading to mitochondrial fission and dysfunction [16,44–46]. None of these phenomena were observed in BTHS cells, in which no OPA-1 complex modification occurred. We therefore, suggest that the fundamental interactions involved in OPA-1 stability mediated by the cardiolipin are not affected in BTHS cells and that these interactions, therefore, remained unchanged in patient-derived cells, regardless of the changes in the mitochondrial compartment. This allows us to speculate on the nature of OPA-1 to cardiolipin relationship which could potentially or not be mediated by the polar head of the cardiolipin (which is unaffected) rather than by the acyl chains (which are more saturated).

4.3. Apoptotic platform formation cannot occur in BTHS cells

Control cells underwent prototypic apoptosis, including caspase-8 activation, a decrease in $\Delta\Psi m$ associated with NAD(P)H oxidation and superoxide anion production followed by caspase-3 activation. In addition, all the expected late events were observed: K^+ efflux, pH changes and aberrant phosphatidyl serine residue exposure at the surface of the plasma membrane (Fig. 7, Table 1). However, all these apoptosis-associated events were abolished in BTHS cells, which were unable to undergo apoptosis via the mitochondrial pathway. Even so, it was important to determine whether some apoptotic pathway unlinked to caspase activation was preserved in these cells

Table 3

Flow cytometry analysis of apoptosis-associated events occurring in control and BTHS lymphoblasts. Lymphoblasts were incubated for 24 h with or without 0.5 mg/ml Fas antibody, and the following were assessed: (a) caspase-3 cleavage activity, measured as DEVD cleavage activity, phosphatidyl serine residue exposure at the outer surface of the plasma membrane (annexin V-FITC binding in the presence of calcium), potassium efflux, evaluated by determining monochlorobimane fluorescence and pH changes based on SNARF-1AM cleavage and fluorescence. The data are expressed as a percentage of cells (%). (b) Reactive oxygen species (superoxide anion) production, detected by HE cleavage in the mean fluorescence channel (F on 256 channel)[a] is given, together with the percentage (%) of viable cells (TO-PRO-3-negative cells)[b].

Conditions (% cells)	Control 037	Control 037 + Fas	Patient 105-3	Patient 105-3 + Fas
a				
Caspase-3$^+$	6 ± 3	62 ± 3	5 ± 3	15 ± 3
Annexin V$^+$	12 ± 2	65 ± 3	9 ± 2	12 ± 2
K$^+$ low	6 ± 2	51 ± 4	4 ± 3	9 ± 4
pH (intracellular)	7.4 ± 0.1	6.9 ± 0.1	7.4 ± 0.1	7.4 ± 0.1
b				
HE$^+$ (% cells)	3 ± 2	60 ± 3	9 ± 2	14 ± 2
HE (mean F^a of viable cells)	8.4 ± 1.2^a (97%)^b	10.1 ± 1.2^a (40%)^b	**16 ± 0.9^a** **(81%)**^{b}	18 ± 0.9^a (76%)^b

The bold emphasis the value determined for the patient.

Table 4

Caspase-8 binding to mitochondria from control and BTHS lymphoblasts. After lymphoblasts were incubated for 8 h with or without 0.5 mg/ml Fas antibody, mitochondria where extracted and purified. FAM-LETD-fmk was incubated with isolated mitochondria for 1 h at 37 °C, and the mitochondria were then washed twice in respiratory buffer and analyzed by flow cytometry. As a control, mitochondria were first incubated for 15 min at 37 °C with the caspase-8 inhibitor Z-IETD-fmk (50 μM) or the pan-caspase inhibitor Q-VD-OPH (10 μM, which has the advantage of not affecting cathepsin and calpain activities) and then incubated with FAM-LETD-fmk, which binds to the catalytic site of caspase-8 if this enzyme is present at the mitochondrial surface. The data are expressed as mean fluorescence values (mean F, arbitrary units, a.u.) for a cell population subjected to the treatment concerned. The control values correspond to autofluorescence.

Conditions	Control mitochondria (mean F, a.u.)	BTHS mitochondria (mean F, a.u.)
Control	8.9 ± 1.1	8.7 ± 1.0
FAM-LETD-fmk	87.5 ± 1.9	13.9 ± 2.0
FAM-LETD-fmk + Z-IETD-fmk	12.7 ± 1.8	9.8 ± 1.8
FAM-LETD-fmk + Q-VD-OPH	12.9 ± 2.0	11.2 ± 1.9

after Fas ligation, dead domain aggregation and pre-activation of capase-8.

When present (i.e., introduced intracellularly by square pulsed electropermeabilization), tBid induced a higher rate of apoptosis in BTHS cells than in controls (Fig. 8A), undoubtedly due to the higher MLCL content of these cells (Fig. 2). Consistent with this observation, tBid has been reported to have a high affinity for MLCL [47]. These results indicate that apoptosis in BTHS cells is blocked at the level of tBid production (resulting in an absence of the activation platform usually formed by caspase-8/Bid and mature CL), suggesting that this process may be strictly related to caspase-8 activity at the mitochondrial platform [15]. Active caspase-8 binding to mitochondria seemed to be affected in BTHS cells (Table 4), as we detected no binding of FAM-LETD-fmk

to BTHS mitochondria, whereas the control cells displayed FAM-LETD-fmk fluorescence associated with the binding of active caspase-8 to mitochondria. Overall, these results confirm previous findings that a caspase-8/Bid/cardiolipin platform is generated at mitochondrial contact sites but that this platform cannot form in the presence of modified CL, as in BTHS cells [15]. It has also been proposed that the absence of platform formation simply reflects the reduced amount of CL in Barth syndrome. This is inconsistent with our observation that the low level of CL in CLS1 knockdown HeLa cells does not lead to an inhibition of apoptosis but actually accelerates it (the platform is formed and tBid is produced, and it is able to interact efficiently with the remaining CL) towards secondary necrosis [14].

4.4. BTHS cells may be more sensitive to stress

The cardiolipin metabolism defect associated with Barth syndrome manifests as CL depletion, MLCL accumulation and CL species diversification, resulting in the generation of CL molecules with different
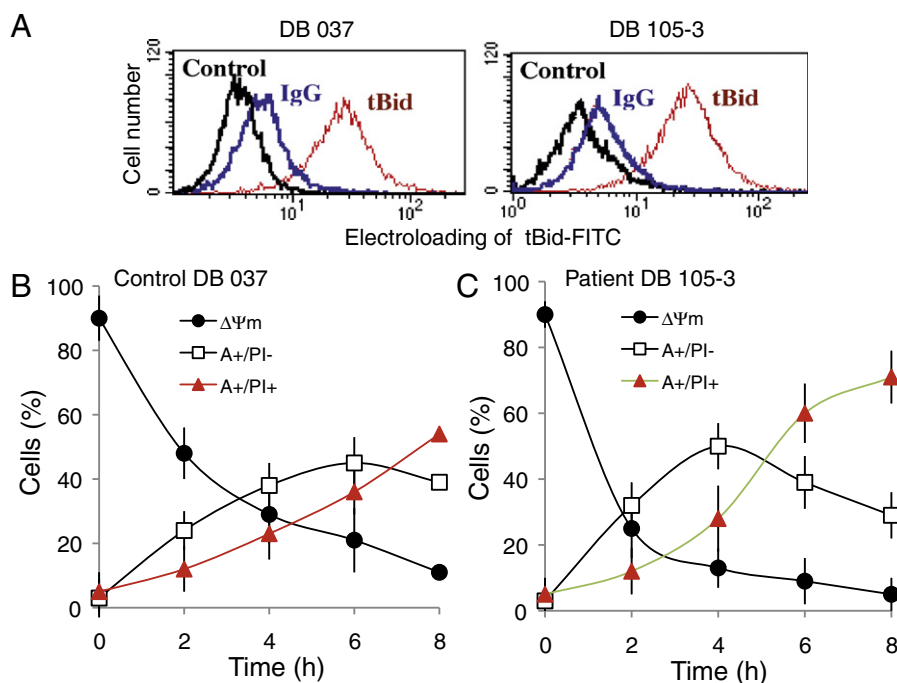

Fig. 8. Electropermeabilization by tBid in control and BTHS lymphoblasts, demonstrating their ability to undergo tBid-mediated cell death. (A) FITC-fluorescence of cells electroloaded with tBid-FITC (similar efficiency for the two cell lines). (B) Measurement of the decrease in mitochondrial membrane potential and cell death induced by tBid electroloading in control lymphoblasts (DB037). (C) Measurement of the decrease in mitochondrial membrane potential and cell death induced by tBid electroloading in patient lymphoblasts (DB105-3).

fatty acyl compositions [3,41,48,49]. It remains unclear whether and how abnormal CL homeostasis actually plays a role in the pathogenesis of Barth syndrome.

Our findings highlight major effects of CL depletion and changes to acyl chain composition in the remaining CL on the structure and functions of mitochondria in the lymphoblasts of BTHS patients. These alterations are almost entirely compensated at the cellular level, in terms of bioenergetics, by an increase in mitochondrial mass. They are, therefore, unlikely to have a profound impact on cell fate in the short term. However, cells from patients may be more sensitive to stress and to long-term micro-destabilization, because the only remarkable characteristic of these cells observed here was a higher basal level of superoxide anion production (Table 3). This characteristic has been previously described in the yeast *taz1Δ* mutant, which exhibits an increased protein carbonylation, an indicator of reactive oxygen species (ROS) [50]. These results suggest that yeast cell mutant models might be very useful to decipher some pathways which might have been conserved from yeast to mammals [51]. Thus, although conditions differ markedly between tissues, affected tissues may be more sensitive to the destabilization of their environment and to stress.

Mitochondrial dysfunction and the inhibition of proapoptotic signaling via mitochondria may cooperate in disease pathogenesis. Effectively, the extrinsic, or death receptor pathway integrates apoptotic signals via caspase-8. The non-apoptotic functions of caspase-8 include an essential role in hematopoiesis and lymphocyte clonal expansion, and the tempering of autophagy in T cells. The catalysis-competent form of caspase-8 is required for rapid T-cell proliferation in response to TCR activation, but caspase-8 processing is required only to promote apoptosis [52]. The pathologic effects of the accumulation of uncleaved caspase-8 are unknown, and will present a challenge in the development of new treatments. Furthermore, questions remain about whether the lack of activation of this specific apoptotic pathway, which is required for normal cell function, is of importance in Barth syndrome lymphocytes and whether it may lead to an increase in inflammation, because other cell death-inducing pathways not requiring caspase-8 activation are conserved.

Questions also remain concerning similarities to Barth syndrome neutrophils. The mitochondria of neutrophils from patients with Barth syndrome, despite their almost exclusive role in glycolysis, have several impairments in common with lymphoblast mitochondria [1]. The respiratory chain is disrupted in neutrophils: electrons are received by complex III, but seem to be transferred rarely, if at all, to complex IV and then to molecular oxygen to generate H_2O. Instead, electrons may be transferred directly to oxygen in complex III, increasing the production of reactive oxygen species (ROS), which may have potentially harmful effects or may, alternatively, form part of as yet undiscovered signaling cascades in neutrophils [1]. An evaluation of the potential value of antioxidant treatments would be useful, particularly given the high levels of superoxide production by Barth syndrome lymphocytes (Table 3) and the clinical trials currently underway concerning the use of coenzyme Q10 in other mitochondriopathies (NIH, USA, Phase III trials of Coenzyme Q10 for mitochondrial diseases).

Future therapeutic interventions might also be based on the restoration of CL levels and fatty acid composition. One promising possibility concerns inhibition of the Ca^{2+}-dependent iPLA2-Via. The mature acyl chain composition of CL is determined by a remodeling process that is dependent on *tafazzin*. *Tafazzin* catalyzes phospholipid–lysophospholipid transacylation, a process involving both the deacylation of CL and the reacylation of MLCL. Unlike the CoA-dependent deacylation–reacylation cycle, this process does not require acylCoA, instead it involves the direct transfer of a fatty acid chain from a phospholipid to a lysophospholipid, without the need for phospholipase A_2 and without the generation of free fatty acid [53]. Nevertheless, a Ca^{2+}-dependent phospholipase A_2 (PLA$_2$-VIA) does play a major role in this process, because this enzyme, which is not required for cardiolipin remodeling [53], seems to have a central function in the absence of taffazin or in situations in which *tafazzin* is nonfunctional [54], leading to CL depletion and the accumulation of MLCL. The Ca^{2+}-independent iPLA$_2$-VIA has been implicated in diverse biological processes, including phospholipid remodeling, arachidonic acid release, apoptosis and store-operated Ca^{2+} entry [55]. In addition, iPLA$_2$-VIA knockout mice develop age-dependent neurological impairment [56,57] and mutations in the iPLA$_2$-VI. A gene has been identified in patients with infantile neuroaxonal dystrophy and neurodegeneration with iron accumulation in the brain [58,59]. It is therefore tempting to focus on the study and development of specific inhibitors of PLA$_2$-VIA and their specific targeting to tissues. The recent description of a mouse model of Barth syndrome will also greatly facilitate work in this area [54].

4.5. Summary

In summary, our findings provide new insight into the pathogenesis of BTHS, by highlighting the role played by CL-containing microdomains at mitochondrial contact sites, as *tafazzin* mutation lead to an impairment of *tafazzin* function and the production of smaller amounts of CL with modified acyl chains and the accumulation of monolysocardiolipin, resulting in the impairment of the pro-apoptotic signal. This highlights the importance of the non apoptotic functions of caspase-8 and the contribution of mitochondrial bioenergetic failure even in the presence of compensation at the cellular level. One major question for future studies concerns possible changes in autophagic fluxes, because the inhibition of apoptosis may trigger an increase in autophagy, the elimination of unwanted mitochondria and higher superoxide levels.

Acknowledgements

References

[1] T.W. Kuijpers, N.A. Maianski, A.T. Tool, K. Becker, B. Plecko, F. Valianpour, R.J. Wanders, R. Pereira, J. Van Hove, A.J. Verhoeven, D. Roos, F. Baas, P.G. Barth, Neutrophils in Barth syndrome (BTHS) avidly bind annexin-V in the absence of apoptosis, Blood 103 (2004) 3915–3923.

[2] P.G. Barth, F. Valianpour, V.M. Bowen, J. Lam, M. Duran, F.M. Vaz, R.J. Wanders, X-linked cardioskeletal myopathy and neutropenia (Barth syndrome): an update, Am. J. Med. Genet. A 126 (2004) 349–354.

[3] M. Schlame, M. Ren, Barth syndrome, a human disorder of cardiolipin metabolism, FEBS Lett. 580 (2006) 5450–5455.

[4] S. Bione, P. D'Adamo, E. Maestrini, A.K. Gedeon, P.A. Bolhuis, D. Toniolo, A novel X-linked gene, G4.5. is responsible for Barth syndrome, Nat. Genet. 12 (1996) 385–389.

[5] P. Vreken, F. Valianpour, L.G. Nijtmans, L.A. Grivell, B. Plecko, R.J. Wanders, P.G. Barth, Defective remodeling of cardiolipin and phosphatidylglycerol in Barth syndrome, Biochem. Biophys. Res. Commun. 279 (2000) 378–382.

[6] F.M. Vaz, R.H. Houtkooper, F. Valianpour, P.G. Barth, R.J. Wanders, Only one splice variant of the human *TAZ* gene encodes a functional protein with a role in cardiolipin metabolism, J. Biol. Chem. 278 (2003) 43089–43094, (Epub 42003 Aug 43020).

[7] Y. Xu, R.I. Kelley, T.J. Blanck, M. Schlame, Remodeling of cardiolipin by phospholipid transacylation, J. Biol. Chem. 278 (2003) 51380–51385.

[8] Y. Xu, A. Malhotra, M. Ren, M. Schlame, The enzymatic function of *tafazzin*, J. Biol. Chem. 281 (2006) 39217–39224.

[9] M. Schlame, D. Rua, M.L. Greenberg, The biosynthesis and functional role of cardiolipin, Prog. Lipid Res. 39 (2000) 257–288.

[10] D. Ardail, J.P. Privat, M. Egret-Charlier, C. Levrat, F. Lerme, P. Louisot, Mitochondrial contact sites. Lipid composition and dynamics, J. Biol. Chem. 265 (1990) 18797–18802.

[11] R.H. Houtkooper, F.M. Vaz, Cardiolipin, the heart of mitochondrial metabolism, Cell. Mol. Life Sci. 65 (2008) 2493–2506.

[12] M. Zhang, E. Mileykovskaya, W. Dowhan, Gluing the respiratory chain together: cardiolipin is required for supercomplex formation in the inner mitochondrial membrane, J. Biol. Chem. 2 (2002) 2.

[13] M. Schlame, M. Ren, The role of cardiolipin in the structural organization of mitochondrial membranes, Biochim. Biophys. Acta 1788 (2009) 2080–2083.

[14] S.Y. Choi, F. Gonzalvez, G.M. Jenkins, C. Slomianny, D. Chretien, D. Arnoult, P.X. Petit, M.A. Frohman, Cardiolipin deficiency releases cytochrome c from the inner mitochondrial membrane and accelerates stimuli-elicited apoptosis, Cell Death Differ. 14 (2007) 597–606.

[15] F. Gonzalvez, Z.T. Schug, R.H. Houtkooper, E.D. Mackenzie, D.G. Brooks, R.J. Wanders, P.X. Petit, F.M. Vaz, E. Gottlieb, Cardiolipin provides an essential activating platform for caspase-8 on mitochondria, J. Cell Biol. 183 (2008) 681–696.

[16] R.M. DeVay, L. Dominguez-Ramirez, L.L. Lackner, S. Hoppins, H. Stahlberg, J. Nunnari, Coassembly of Mgm1 isoforms requires cardiolipin and mediates mitochondrial inner membrane fusion, J. Cell Biol. 186 (2009) 793–803.

[17] T. Ban, J.A. Heymann, Z. Song, J.E. Hinshaw, D.C. Chan, OPA1 disease alleles causing dominant optic atrophy have defects in cardiolipin-stimulated GTP hydrolysis and membrane tubulation, Hum. Mol. Genet. 19 (2010) 2113–2122.

[18] A.S. Rambold, J. Lippincott-Schwartz, Mechanisms of mitochondria and autophagy crosstalk, Cell Cycle 10 (2011) 4032–4038.

[19] M. Schlame, D. Acehan, B. Berno, Y. Xu, S. Valvo, M. Ren, D.L. Stokes, R.M. Epand, The physical state of lipid substrates provides transacylation specificity for tafazzin, Nat. Chem. Biol. 8 (2012) 862–869.

[20] C. Kantari, H. Walczak, Caspase-8 and bid: caught in the act between death receptors and mitochondria, Biochim. Biophys. Acta 1813 (2011) 558–563.

[21] Z.T. Schug, F. Gonzalvez, R.H. Houtkooper, F.M. Vaz, E. Gottlieb, BID is cleaved by caspase-8 within a native complex on the mitochondrial membrane, Cell Death Differ. 18 (2011) 538–548.

[22] Y. Xu, J.J. Sutachan, H. Plesken, R.I. Kelley, M. Schlame, Characterization of lymphoblast mitochondria from patients with Barth syndrome, Lab. Invest. 85 (2005) 823–830.

[23] J. Johnston, R.I. Kelley, A. Feigenbaum, G.F. Cox, G.S. Iyer, V.L. Funanage, R. Proujansky, Mutation characterization and genotype–phenotype correlation in Barth syndrome, Am. J. Hum. Genet. 61 (1997) 1053–1058.

[24] F. Valianpour, R.J. Wanders, H. Overmars, P. Vreken, A.H. Van Gennip, F. Baas, B. Plecko, R. Santer, K. Becker, P.G. Barth, Cardiolipin deficiency in X-linked cardioskeletal myopathy and neutropenia (Barth syndrome, MIM 302060): a study in cultured skin fibroblasts, J. Pediatr. 141 (2002) 729–733.

[25] O. Seksek, N.H. Toulmé, F. Sureau, J. Bolard, SNARF-1 as an intracellular pH indicator in laser microspectrometry, a critical assessment, J. Anal. Biochem. 193 (1991) 49–54.

[26] J.A. Thomas, R.N. Buschbaum, A. Zimniak, E. Racker, Intracellular pH measurement in Ehrlich ascite tumor cells utilizing spectroscopic probes generated in situ, Biochemistry 18 (1979) 2210–2218.

[27] B. Gabriel, F. Sureau, M. Casselyn, J. Teissie, P.X. Petit, Retroactive pathway involving mitochondria in electroloaded cytochrome c-induced apoptosis. Protective properties of Bcl-2 and Bcl-XL, Exp. Cell Res. 289 (2003) 195–210.

[28] M.C. Gendron, N. Schrantz, D. Metivier, G. Kroemer, Z. Maciorowska, F. Sureau, S. Koester, P.X. Petit, Oxidation of pyridine nucleotides during Fas- and ceramide-induced apoptosis in Jurkat cells: correlation with changes in mitochondria, glutathione depletion, intracellular acidification and caspase 3 activation, Biochem. J. 353 (2001) 357–367.

[29] T. Bourgeron, D. Chretien, A. Rötig, A. Munnich, P. Rustin, Isolation and characterization of mitochondria from human B lymphoblastoid cell lines, Biochem. Biophys. Res. Commun. 186 (1992) 16–23.

[30] C. Vives-Bauza, L. Yang, G. Manfredi, Assay of mitochondrial ATP synthesis in animal cells and tissues, Methods Cell Biol. 80 (2007) 155–171.

[31] M. D'Aurelio, F. Pallotti, A. Barrientos, C.D. Gajewski, J.Q. Kwong, C. Bruno, M.F. Beal, G. Manfredi, In vivo regulation of oxidative phosphorylation in cells harboring a stop-codon mutation in mitochondrial DNA-encoded cytochrome c oxidase subunit I, J. Biol. Chem. 276 (2001) 46925–46932.

[32] I.A. Trounce, Y.L. Kim, A.S. Jun, D.C. Wallace, Assessment of mitochondrial oxidative phosphorylation in patient muscle biopsies, lymphoblasts, and transmitochondrial cell lines, Methods Enzymol. 264 (1996) 484–509.

[33] A. Olichon, L.J. Emorine, E. Descoins, L. Pelloquin, L. Brichese, N. Gas, E. Guillou, C. Delettre, A. Valette, C.P. Hamel, B. Ducommun, G. Lenaers, P. Belenguer, The human dynamin-related protein OPA1 is anchored to the mitochondrial inner membrane facing the inter-membrane space, FEBS Lett. 523 (2002) 171–176.

[34] T. Landes, L.J. Emorine, D. Courilleau, M. Rojo, P. Belenguer, L. Arnaure-Pelloquin, The BH3-only Bnip3 binds to the dynamin Opa1 to promote mitochondrial fragmentation and apoptosis by distinct mechanisms, EMBO Rep. 11 (2010) 459–465.

[35] M. D'Aurelio, C.D. Gajewski, G. Lenaz, G. Manfredi, Respiratory chain supercomplexes set the threshold for respiration defects in human mtDNA mutant cybrids, Hum. Mol. Genet. 15 (2006) 2157–2169.

[36] C. Frezza, S. Cipolat, O. Martins de Brito, M. Micaroni, G.V. Beznoussenko, T. Rudka, D. Bartoli, R.S. Polishuck, N.N. Danial, B. De Strooper, L. Scorrano, OPA1 controls apoptotic cristae remodeling independently from mitochondrial fusion, Cell 126 (2006) 177–189.

[37] R. Yamaguchi, L. Lartigue, G. Perkins, R.T. Scott, A. Dixit, Y. Kushnareva, T. Kuwana, M.H. Ellisman, D.D. Newmeyer, Opa1-mediated cristae opening is Bax/Bak and BH3 dependent, required for apoptosis, and independent of Bak oligomerization, Mol. Cell 31 (2008) 557–569.

[38] F.C. Kischkel, S. Hellbardt, I. Behrmann, M. Germer, M. Pawlita, P.H. Krammer, M.E. Peter, Cytotoxicity-dependent Apo-1 (FAs/CD95)-associated proteins form a death-inducing signaling complex (DISC) with the receptor, EMBO J. 14 (1995) 5579–5588.

[39] H. Zou, Y. li, X. Liu, X. Wang, An APAF-1.cytochrome c multimeric complex is a functional apoptososome that activates procaspase-9, J. Biol. Chem. 274 (1999) 11549–11556.

[40] J.S. Ingwall, R.G. Weiss, Is the failing heart energy starved? On using chemical energy to support cardiac function, Circ. Res. 95 (2004) 135–145.

[41] E. Schafer, N.A. Dencher, J. Vonck, D.N. Parcej, Three-dimensional structure of the respiratory chain supercomplex I1III2IV1 from bovine heart mitochondria, Biochemistry 46 (2007) 12579–12585.

[42] M. McKenzie, M. Lazarou, D.R. Thorburn, M.T. Ryan, Mitochondrial respiratory chain supercomplexes are destabilized in Barth Syndrome patients, J. Mol. Biol. 361 (2006) 462–469.

[43] D. Acehan, Y. Xu, D.L. Stokes, M. Schlame, Comparison of lymphoblast mitochondria from normal subjects and patients with Barth syndrome using electron microscopic tomography, Lab. Invest. 87 (2007) 40–48.

[44] S. Duvezin-Caubet, R. Jagasia, J. Wagener, S. Hofmann, A. Trifunovic, A. Hansson, A. Chomyn, M.F. Bauer, G. Attardi, N.G. Larsson, W. Neupert, A.S. Reichert, Proteolytic processing of OPA1 links mitochondrial dysfunction to alterations in mitochondrial morphology, J. Biol. Chem. 281 (2006) 37972–37979.

[45] L. Griparic, T. Kanazawa, A.M. van der Bliek, Regulation of the mitochondrial dynamin-like protein Opa1 by proteolytic cleavage, J. Cell Biol. 178 (2007) 757–764.

[46] Z. Song, H. Chen, M. Fiket, C. Alexander, D.C. Chan, OPA1 processing controls mitochondrial fusion and is regulated by mRNA splicing, membrane potential, and Yme1L, J. Cell Biol. 178 (2007) 749–755.

[47] M.D. Esposti, I.M. Cristea, S.J. Gaskell, Y. Nakao, C. Dive, Proapoptotic bid binds to monolysocardiolipin, a new molecular connection between mitochondrial membranes and cell death, Cell Death Differ. 10 (2003) 1300–1309.

[48] A. Malhotra, I. Edelman-Novemsky, Y. Xu, H. Plesken, J. Ma, M. Schlame, M. Ren, Role of calcium-independent phospholipase A2 in the pathogenesis of Barth syndrome, Proc. Natl. Acad. Sci. U. S. A. 106 (2009) 2337–2341.

[49] M.A. van Werkhoven, D.R. Thorburn, A.K. Gedeon, J.J. Pitt, Monolysocardiolipin in cultured fibroblasts is a sensitive and specific marker for Barth syndrome, J. Lipid Res. 47 (2006) 2346–2351.

[50] S. Chen, Q. He, M.L. Greenberg, Loss of tafazzin in yeast leads to increased oxidative stress during respiratory growth, Mol. Microbiol. 68 (2008) 1061–1072.

[51] Z. Gu, F. Valianpour, S. Chen, F.M. Vaz, G.A. Hakkaart, R.J. Wanders, M.L. Greenberg, Aberrant cardiolipin metabolism in the yeast taz1 mutant: a model for Barth syndrome, Mol. Microbiol. 51 (2004) 149–158.

[52] S. Leverrier, G.S. Salvesen, C.M. Walsh, Enzymatically active single chain caspase-8 maintains T-cell survival during clonal expansion, Cell Death Differ. 18 (2011) 90–98.

[53] M. Schlame, Cardiolipin synthesis for the assembly of bacterial and mitochondrial membranes, J. Lipid Res. 49 (2008) 1607–1620.

[54] M.S. Soustek, D.J. Falk, C.S. Mah, M.J. Toth, M. Schlame, A.S. Lewin, B.J. Byrne, Characterization of a transgenic short hairpin RNA-induced murine model of tafazzin deficiency, Hum. Gene Ther. 22 (2011) 865–871.

[55] R.H. Schaloske, E.A. Dennis, The phospholipase A2 superfamily and its group numbering system, Biochim. Biophys. Acta 1761 (2006) 1246–1259.

[56] K. Shinzawa, H. Sumi, M. Ikawa, Y. Matsuoka, M. Okabe, S. Sakoda, Y. Tsujimoto, Neuroaxonal dystrophy caused by group VIA phospholipase A2 deficiency in mice: a model of human neurodegenerative disease, J. Neurosci. 28 (2008) 2212–2220.

[57] I. Malik, J. Turk, D.J. Mancuso, L. Montier, M. Wohltmann, D.F. Wozniak, R.E. Schmidt, R.W. Gross, P.T. Kotzbauer, Disrupted membrane homeostasis and accumulation of ubiquitinated proteins in a mouse model of infantile neuroaxonal dystrophy caused by PLA2G6 mutations, Am. J. Pathol. 172 (2008) 406–416.

[58] S. Khateeb, H. Flusser, R. Ofir, I. Shelef, G. Narkis, G. Vardi, Z. Shorer, R. Levy, A. Galil, K. Elbedour, O.S. Birk, PLA2G6 mutation underlies infantile neuroaxonal dystrophy, Am. J. Hum. Genet. 79 (2006) 942–948.

[59] N.V. Morgan, S.K. Westaway, J.E. Morton, A. Gregory, P. Gissen, S. Sonek, H. Cangul, J. Coryell, N. Canham, N. Nardocci, G. Zorzi, S. Pasha, D. Rodriguez, I. Desguerre, A. Mubaidin, E. Bertini, R.C. Trembath, A. Simonati, C. Schanen, C.A. Johnson, B. Levinson, C.G. Woods, B. Wilmot, P. Kramer, J. Gitschier, E.R. Maher, S.J. Hayflick, PLA2G6, encoding a phospholipase A2, is mutated in neurodegenerative disorders with high brain iron, Nat. Genet. 38 (2006) 752–754.